Implementation requirements for Gbit/s optical receivers with Turbo detection and LDPC decoding

Klaus Oestreich, Joachim Speidel

Universität Stuttgart, Institut für Nachrichtenübertragung, 70569 Stuttgart
E-Mail: klaus.oestreich@inue.uni-stuttgart.de

Abstract

In this paper, we investigate realization aspects of Turbo detection and LDPC decoding for an intensity modulated and direct detected optical transmission link. Target is to find dedicated LDPC codes with overhead of 6.7 % to 14.3 %. Furthermore the influence of quantization is examined. The BER analysis is based on a sophisticated channel model using analytical computation of the branch metrics. It turns out, that an LDPC code of code rate $R_c = 0.889$ and codeword length N in the range of 9000 bits is most suitable. Sampling of the electrial receive signal requires a resolution of the ADC of 5 to 6 bit. In combination with word lengths of 8 bit at the receiver a performance close to the ideal receiver without any quantization can be achieved.

1 Introduction

To cope with the ever increasing data traffic in the internet optical communication systems with high bit rates are required. These high bit-rate transmission systems are affected by signal distortions like chromatic dispersion (CD), polarisation mode dispersion (PMD) and noise. In order to detect the transmitted information correctly, powerful receivers are necessary. Turbo equalization [1] as a combined approach of equalization and decoding has proven to own a considerable performance [2], [3]. In combination with the Bahl-Cocke-Jelinek-Raviv (BCJR) maximum a posteriori (MAP) soft-in soft-out (SISO) equalizer for detection and an iterative Low-Density Parity-Check (LDPC) SISO decoder [4] for forward error correction (FEC) such a receiver can reach the rate-distortion limit with a small gap of only 0.7 dB [5]. In this paper we present implementation requirements for binary intensity modulation (IM) transmission in combination with direct optical photo-detection (DD) which operate close to these limits.

For optical transmission systems codes with high code rate are feasible, as they do not extend the signal bandwidth aggressively. Furthermore the codes shall offer a good compromise between high error correction performance and complexity. For a digital realization of the Turbo equalizer the selection of a specific LDPC code plays an important role. Therefore we present some promising codes.

A real-world solution should operate digitally on sampled and quantized input signals. In addition the arithmetic operations of the equalizer and decoder can only be processed with a limited word length. A poor resolution of the Analog-to-Digital Converter (ADC) as well as insufficient word lengths reduce the performance of the receiver. By the use of computer simulations we can show which resolution of the ADC and which word length of the operations of the detector and decoder are required.

This paper is organized as followes. In section 2 Turbo equalization and the system model is introduced. Section 3 provides a brief overview of LDPC codes and points out some promising codes for Turbo equalization. The impact of sampling and quantization is investigated in section 4, and section 5 concludes the paper.

2 Receiver Structure and System Model

2.1 Detection and Decoding

The investigated Turbo equalizer consist of the well-known BCJR equalizer for detection and an iterative sum product algorithm (SPA) decoder. As shown in Fig. 1 no interleaver and deinterleaver are necessary for LDPC coded Turbo equalizers which is advantageous with respect to implementation complexity.

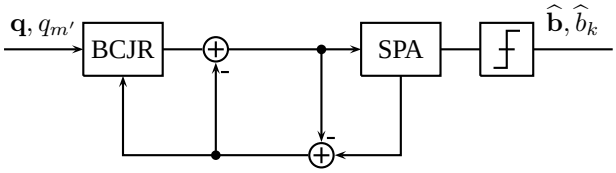

Fig. 1: Block diagram of the Turbo equalizer with BCJR detection and SPA decoder.

2.1.1 BCJR equalizer and its implementation

The BCJR algorithm [6] is a Trellis based MAP symbol-by-symbol (sbs) estimation and minimizes the bit error probability (BER). It delivers the a posteriori probability ratio

$$L\left(a_m|\mathbf{q}\right) = \ln \frac{P\left[a_m = 1|\mathbf{q}\right]}{P\left[a_m = 0|\mathbf{q}\right]} \tag{1}$$

based on the input sequence $\mathbf{q}$. This sequence contains the transmitted bits which are distorted by inter-symbol-interference (ISI) and noise.

The computation of the likelihood values for the individual symbols can be subdivided into five steps: the branch metric computation based on the probability density functions (pdfs) of the sequence $\mathbf{q}$, the forward and backward metric computation, storing of intermediate results and the computation of the estimates for each symbol. Required mathematical operations are exponential as well as logarithmic functions.

For a hardware implementation the so called JACLOG or MAXLOG version [7] using the "Jacobian logarithm" is advantageous as they simplify the operations. Though the forward and backward computation of the pathmetrics is still a bottleneck for these equalizers. As the pathmetrics converge with the aquisition depth towards reliable values, the input sequence can be sub-divided into severeal parallel windows. For each window the a posteriori values can be computed simultaneously. Thus the equalizer is scalable with respect to the throughput. By proper selection of the number and width of the windows, bitrates of 10 Gbit/s and more are achievable [8], [9].

2.1.2 Sum product algorithm

The SPA decoder is an iterative SISO decoder which is based on the Tanner graph. It uses the extrinsic information of the equalizer for further error correction. In each iteration, information is passed between the variable- and the checknodes. Every node offers a calculation rule in order to combine the incomming signals. In this way, the reliability of each bit of the codeword is improved from iteration to iteration. A detailed description of the SPA can be found in [10]. As the SPA is based on the Tanner graph, parallel computation in the nodes [11] and thus high data rates are possible.

2.1.3 Further implementation aspects

The Turbo equalizer according to Fig. 1 contains a feedback loop from the decoder to the equalizer. By exchanging extrinsic information between the equalizer and the FEC decoder the performance can be improved for each iteration. In [5] the authors compare a Turbo equalizer with 10 Turbo equalizer iterations and 10 SPA iterations with the concatenation of a BCJR equalizer and an SPA decoder with 25 iterations. It is shown, that the concatenation of detection and decoding is only a tenth of a dB worse than the Turbo equalizer. All investigations in this paper are therefore based on this receiver without feedback loop as it has a lower complexity.

2.2 System Model

Fig. 2(a) shows the block diagram of the fiber optic transmission link. The system consists of the transmitter (TX) a standard single mode fiber (SSMF) and the optically preamplified receiver (RX). The equivalent lowpass representation of the transmission system according to Fig. 2(b) exhibits the same input/output relation as the bandpass model.

At the transmitter side the encoder adds redundancy to a block of K information bits b_k in order to get a block of N binary symbols a_m. Thus the bit rate R_b is enlarged by the reciprocal code rate R_c^{-1} and the symbol rate on the fiber is

$$R_s = \frac{R_b}{R_c}. \tag{2}$$

The net information bit rate is fixed to 10 Gbit/s.

The binary symbols a_m are externally modulated by a chirp-free absorption modulator (EAM) onto the output signal of a continuous wave (CW) laser with mean power P_{cw}. The lowpass equivalent of this intensity modulated optical field at the output of the transmitter is

$$\overrightarrow{s\,(t)} = \vec{e}\sqrt{\sum_{m=-\infty}^{\infty} a'_m P_{cw}\, g\,(t - mT_s)} \tag{3}$$

and exhibits two polarization directions: $\overrightarrow{s(t)} = [s_x(t), s_y(t)]^T$. In equ. (3) $\vec{e} = [e_x, e_y]^T$ is the polarization Jones vector with $\|\vec{e}\|^2 = 1$, a'_m are the transmit symbols including the extinction ratio of the modulator and $g\,(t)$ is the impulse response of the pulse shaper.

The signal propagation in the SSMF is modeled as a pair of nonlinearly coupled nonlinear Schrödinger equations according to [12]. It considers intersymbol interference (ISI) due to chromatic dispersion (CD), polarization mode dispersion (PMD) of 1st and 2nd order as well as the loss of the fiber α_{loss}. The nonlinear fiber transfer function $\underline{\overrightarrow{b\,[\cdot]}}$ describes this signal propagation.

At the receiver an erbium doped fiber amplifier (EDFA) with attenuation G fully compensates the loss of the fiber. This amplifier is the major source of noise in the system and adds the amplified spontaneous emission (ASE) noise $\overrightarrow{n(t)}$ (a two dimensional complex valued Gaussian noise process) to the signal. Before the detection of the signal by the photo diode, it is filtered by the optical filter $\mathbf{h}_o(t)$. After electrical filtering the analog receive signal is given by

$$q(t) = \frac{1}{2}\eta \left\| \mathbf{h}_o(t) * \left(\underline{\overrightarrow{b\left[\overrightarrow{s(t)}\right]}} + \overrightarrow{n(t)} \right) \right\|_2^2 * h_{el}(t), \tag{4}$$

where η is the optoelectronic conversion factor.

For digital signal processing of the receive signal, $q(t)$ is sampled at $t = (m'/l)\,T_s - t_0$, while $m' \in \mathbb{Z}$, $l \in \mathbb{N}$ and $T_s = 1/R_s$ is the symbol interval. The arbitrary time shift t_0 is used for synchronization. The digital representation of the receive signal is

$$q_{m'} = q\left(\frac{m'}{l}T_s - t_0\right). \tag{5}$$

For sampling with $l > 2$ no significant performance improvement can be observed [13]. Therefore we consider the case $l = 2$ with two samples per symbol a_m according to [5].

For detection and decoding the pdfs of the samples $q_{m'}$ are required as branch metrics for the BCJR algorithm. These pdfs are derived by the use of the Karhunen

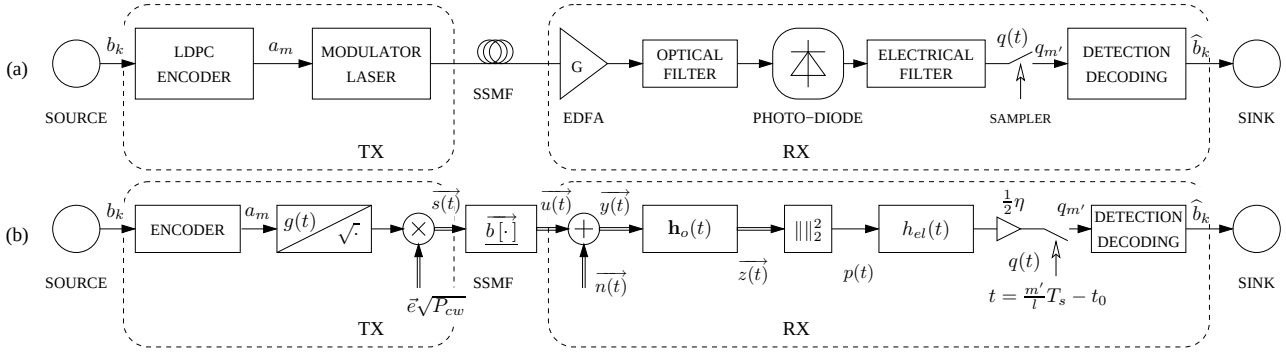

Fig. 2: Fiber optic transmission link with transmitter (TX), a standard single mode fiber (SSMF) and receiver (RX). (a) System model. (b) Equivalent lowpass model.

Loève series expansion (KLSE) and a moment generation function (MGF). A detailed derivation of the pdfs can be found in [5].

The signal to noise ratio (SNR) is definded as the ratio of the symbol energy to the total noise spectral density N_0 of the two dimensional noise process $\overrightarrow{n(t)}$

$$\frac{E_b}{N_0} = \frac{E_S}{N_0}\frac{1}{R_c} = \frac{\frac{1}{2}P_{cw}dT_s}{2N_{0,pol}}\frac{1}{R_c}. \tag{6}$$

E_b is the energy per bit, E_s the symbol energy, $N_{0,pol}$ the spectral density per complex polarization component and d the impulse shaper duty cycle. In optical communication systems very often the optical signal to noise ratio (OSNR) is used as a figure of merit. The OSNR can be derived as

$$\text{OSNR}_{B,dB} = \left.\frac{P_{mean}}{P_{noise,B}}\right|_{dB} = \left.\frac{E_b}{N_0}\right|_{dB} - 10\log\frac{B}{R_b}. \tag{7}$$

B is the measurement bandwidth that is mostly chosen as 12.5 GHz.

3 Finite geometry LDPC-Codes for optical receivers

LDPC codes are linear block codes which are specified by their parity check matrix $\mathbf{H}$. LDPC codes based on Euclidean (EG) and projective geometries (PG) were recently developed [14], [15] and investigated for fiber optic transmission links [4], [16].

The construction of finite geometry LDPC codes is based on lines and points of m-dimensional Euclidian and projective geometries over finite fields. As a result four different classes of finite geometry LDPC codes can be obtained: Type 1 and type 2 Euclidean geometry (EG) LDPC codes as well as type 1 and type 2 projective geometry (PG) LDPC codes. Type 2 codes are derived from the type 1 codes by transposing their parity-check matrix.

Codes determined by use of these geometries are referred to as base codes. By this approach a large variety of LDPC codes with different properties can be obtained. A technique to enlarge the number of codes is shortening of LDPC codes. Deleting $t < c$ of cirulant submatrices of the quasi-cyclic parity check matrix $\mathbf{H}$ results in a new code with different R_c and reduced row weight ρ. Further row and column decomposition can be applied to the parity check matrices by splitting each circulant submatrix into several circulant matrices. Thus extended finite geometry LDPC codes of nearly any code rate can be generated. The performance of the SPA decoder depends very much on cycles of short length in its Tanner graph. By deleting diagonals of ones in $\mathbf{H}$ the number of cycles in the Tanner graph can be reduced.

In order to find suitable LDPC codes we simulated a huge number of base codes, shortened, row and column extended as well as cycle reduced codes of different code rates. We present the codes with the best BER vs. E_b/N_0 for the code rates $R_c = 0.938$, 0.889 and 0.875 in Tab. I. Their geometry G is either Euclidean or projective of type 1 or 2. m and s are parameters of the geometry, c the number of square matrices, ρ the row weight and γ the column weight. For all codes the length of the codeword N and the information word K, the number of parity check bits $N-K$, the number of rows in the parity check matrix J, the code rate $R_c = K/N$ and the code overhead $O_c = 1 - R_c^{-1}$ are given.

In Fig. 3, the required SNR versus differential group delay $\Delta\tau$ [Fig. 3(a)] and residual chromatic dispersion R_D [Fig. 3(b)] is plotted for the LDPC codes of Tab. I. The numerical analysis are based on the optical transmission scheme of section 2 with $R_b = 10\,\text{Gbit/s}$. The impulse $g(t)$ exhibits a cos-square waveform with roll off factor $\alpha = 0.35$ and duty cycle $d = 1$. The power of the laser is $P_{cw} = 3\,\text{dBm}$, the EAM has an extinction ratio of $13\,\text{dB}$, and $\eta = 1$. For the optical filter bandwidth $B_{o,3dB} = 14\,\text{GHz}$ and for the electrical filter cutoff frequency $f_{el,3dB} = 7\,\text{GHz}$ holds. The filters are modeled with Gaussian shape. The number of states in the trellis are always chosen to cover the system memory perfectly. These properties hold also for the other numerical analysis of this paper.

For the sake of simplicity a short hand notation of the codes is chosen in Fig. 3. E.g. EG2m5s2-16of85-shortened indicates a shortened EG-2 code with $m = 5$, $s = 3$ and 16 of 85 submatrizes. For each R_c the best LDPC code has a difference to the system capacity SNR bound smaller than 2 dB for all $\Delta\tau$. The gap is even

TABLE I: Selected LDPC codes

G	m	s	N	K	$N-K$	R_c	O_c	c	ρ	γ	J	extension	
EG-1	2	6	65520	61425	4095	0.938	6.7%	1	64	4	4095	16x column ext.	
EG-2	5	2	16368	15345	1023	0.938	6.7%	16	64	4	1023	-	shortened
EG-2	5	2	32736	30690	2046	0.938	6.7%	32	63	4	2046	2x row ext.	shortened
EG-2	3	3	9198	8176	1022	0.889	12.5%	9	27	3	1022	2x row and 2x column ext.	cycle reduced
EG-2	5	2	9207	8184	1023	0.889	12.5%	9	36	4	1023	-	shortened
EG-2	3	3	8176	7154	1022	0.875	14.3%	8	32	4	1022	2x row and 2x column ext.	shortened
EG-1	2	5	8184	7161	1023	0.875	14.3%	1	28	4	1023	8x column ext.	cycle reduced

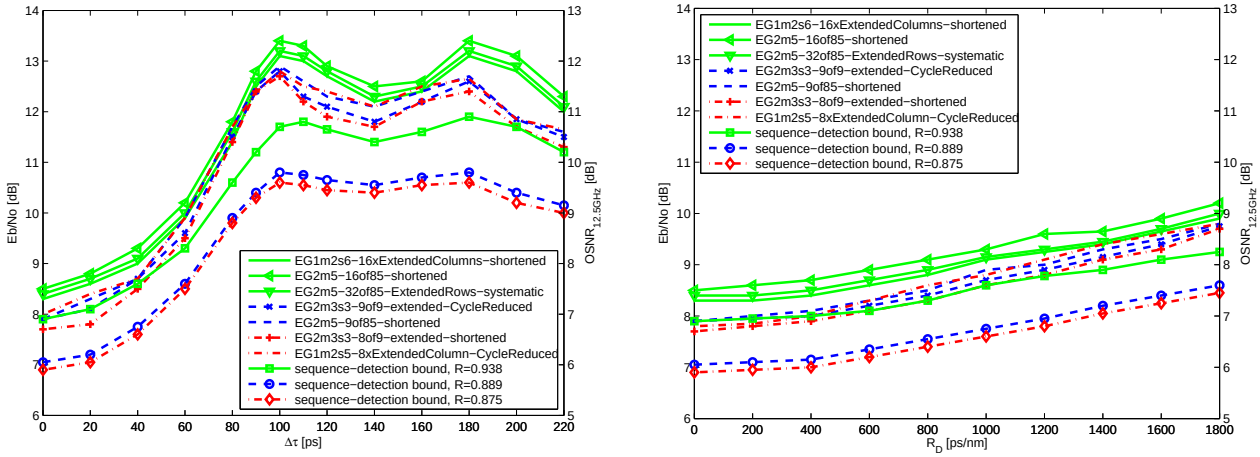

(a) (b)

Fig. 3: Required SNR versus dispersion for a receiver operating at a BER of 10^{-9} and at $R_b = 10\,\mathrm{Gbit/s}$. (a) differential group delay $\Delta\tau$, (b) residual dispersion R_D. As SNR the E_B/N_0 as well as the $\mathrm{OSNR}_{12.5\mathrm{GHz}}$ are given.

smaller for the residual chromatic dispersion R_D. The extended EG-1 $m = 2$, $s = 6$ code performs best of the codes with $R_c = 0.938$. It has the same overhead $O_c = 6.7\%$ as the widely used Reed Solomon (RS) code RS(255,239) that is described in the ITU-T G.975 recommendation. Compared to all other codes it exhibits the smallest gap to its SNR bound.

The best BER vs. E_b/N_0 offers the extended and shortened EG-2 $m = 3$, $s = 3$ code with code overhead $O_c = 14.3\%$. Though the net coding gain of this code is only 0.1 dB - 0.2 dB better than for the cycle reduced version of this code with a lower code overhead of $O_c = 12.5\%$.

The calculation complexity in one checknode of the SPA decoder depends on the row weight ρ of the parity check matrix $\mathbf{H}$. The crucial factor for the complexity of one variablenode is the column weight γ. Comparing the three mentioned codes, the cycle reduced code with $O_c = 12.5\%$ exhibits the lowest complexity for one single variable- and checknode. The total number of variable- and checknodes in the Tanner graph depends on N and J. Thus, for a hardware efficient implementation the EG-1 $m = 2$, $s = 6$ is out off the race. For the two remaining codes the complexity and the performance is comparable but the cycle reduced code is better in terms of code overhead and required symbol rate R_s.

4 Quantization

The performance of the receiver with SISO detection and decoding for high speed optical communications depends very much on the quantization of the received signal and the computational accuracy. This has been neglected so far in order to obtain theoretically optimal results. However, quantization has to be considered in a more realistic model. In the following, we therefore examine the influence of the analog to digital conversion on the performance and necessary word lengths.

4.1 Resolution of the ADC

The analog receive signal $q(t)$ is sampled at equidistant time instances in order to get the digital version $q_{m'}$. For the case $l = 2$ with two samples per symbol the sampling rate is twice the symbol rate R_s. A net bit rate of $R_b = 10\,\mathrm{Gbit/s}$ and a code rate of $R_c = 0.889$ requires a sampling rate of approximately 22.5 GS/s. Current high speed ADCs offer only a limited resolution.

Being restricted to a certain number of output levels of the ADC the quantizer can be optimized using nonuniform step size instead of a uniform quantization. Considering the pdf of the signal amplitude $q(t)$ a feasible nonuniform quantization can be found. The optical received signal exhibits a Gaussian distribution which is transformed into a Chi-square like distribution due to the quadratic behaviour of the photo diode. Let L be the number of output levels and V the upper limit of the signal amplitude. Choosing a uniform distribution of

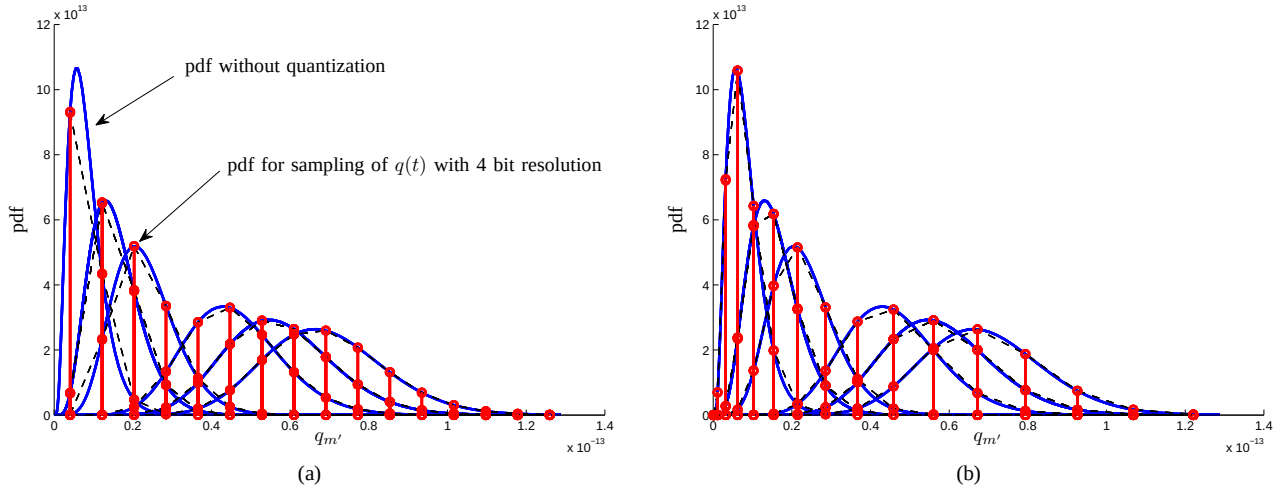

Fig. 4: pdf of $q(t)$ for $R_c = 0.889$, $\Delta\tau = 60\,\mathrm{ps}$ and $R_D = 400\,\mathrm{ps/nm}$ approximated using (a) uniform quantization and (b) nonuniform quantization with a resolution of 4 bits.

the output levels in front of the photo-diode with the quantized values

$$\sqrt{\widetilde{q}_{m'}} = \sqrt{\Delta}\left(\frac{1}{2} + i\right), \qquad i = 0, 1, ...L \tag{8}$$

with step size $\sqrt{\Delta} = \frac{\sqrt{V}}{L}$, the output levels have a nonuniform distribution in the electrical domain. The output levels after photo detection are

$$\widetilde{q}_{m'} = \Delta\left(\frac{1}{2} + i\right)^2 \tag{9}$$

and the step size increases linearly with $2\Delta i$. As can be seen from Fig. 4 the pdf of $q(t)$ is very steep for small sampled values and smooth for larger values. Thus the nonuniform quantization [see Fig. 4(b)] performs better than the uniform quantization [Fig. 4(a)].

Fig. 5 shows the BER versus SNR for different resolutions of the ADC. The fiber link has a differential group delay of $\Delta\tau = 60\,\mathrm{ps}$ and a residual chromatic dispersion of $R_D = 400\,\mathrm{ps/nm}$. For a resolution of 3 bit a gain of 0.5 dB can be achieved by using a nonuniform instead of a uniform resolution. However, the loss due to quantization with 3 bits is greater than 3 dB compared to the ideal case. This is not tolerable.

Tab. II summarizes the SNR-penalty due to quantization for the considered resolutions. A resolution of 5 or 6 bits causes almost no reduction of performance. For a 6 bit resolution a nonuniform quantization induces no gain, thus simpler ADC with uniform quantization can be used instead.

TABLE II: SNR-penalty due to quantization of $q(t)$

resolution	uniform	nonuniform	difference between both q.
3 bit	3.6 dB	3.1 dB	0.5 dB
4 bit	1.0 dB	0.7 dB	0.3 dB
5 bit	0.2 dB	0.1 dB	0.1 dB
6 bit	≈0 dB	≈0 dB	≈0 dB

In Fig. 6, the required SNR versus differential group delay $\Delta\tau$ [Fig. 6(a)] and residual chromatic dispersion

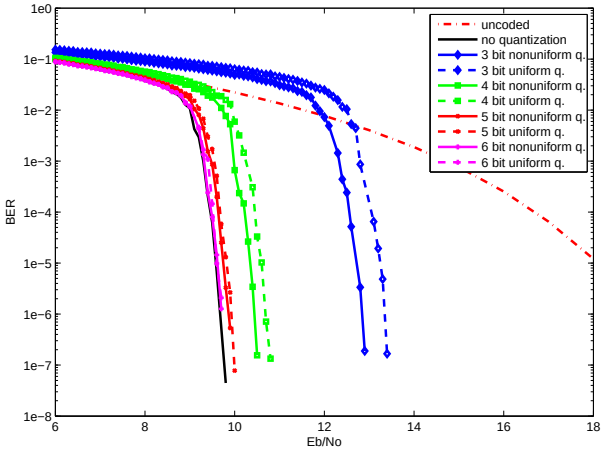

Fig. 5: BER vs. SNR for the EG2m3s3-9of9-ex-CR code using different quantizations of $q(t)$ for $\Delta\tau = 60\,\mathrm{ps}$ and a residual chromatic dispersion of $R_D = 400\,\mathrm{ps/nm}$.

R_D [Fig. 6(b)] is plotted for a resolution of 5 and 6 bits as well as for the ideal case without quantization. It turns out that these resolutions are applicable for all dispersion values.

Analog-to-Digital flash converters in 90 nm CMOS technology with nominal resolution of 6 bits have been reported [17]. Its maximum sampling rate of 25 GS/s is sufficient for our application. Though the effective number of bits (ENOB) which is related to the bandwidth of the input signal is less than 6 bits. The electrical filter at the receiver limits the bandwidth of $q(t)$ to 7 GHz. The ENOB for a sampling rate of 25 GS/s at 7 GHz is approximately 3.5 bits. Thus analog to ditigal conversion is still a limiting factor for high speed optical communication.

4.2 Required word length

Apart from the resolution of the ADC the computational accuracy of the arithmetic operations of the equalizer and the decoder exerts influence onto the performance of the

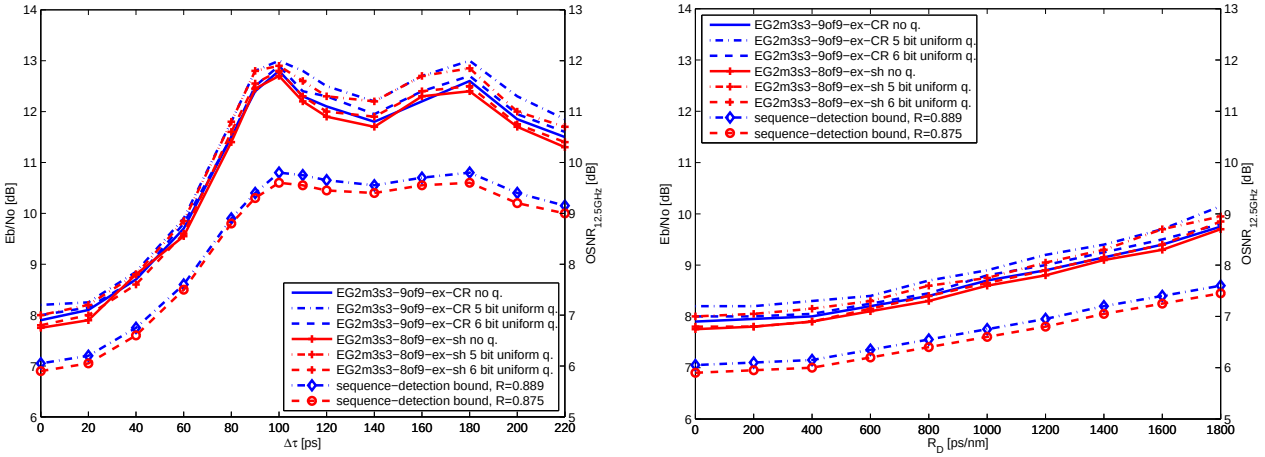

Fig. 6: Required SNR versus dispersion for a receiver operating at a BER of 10^{-9} and at $R_b = 10\,\mathrm{Gbit/s}$ for quantization with different resolutions. (a) PMD, (b) CD.

receiver. Fig. 7 compares BER vs. SNR for word lengths of the signals of 7 to 16 bit assuming an ADC resolution of 6 bit. As number format a fixpoint representation is used. As can be seen, for a word length of 7 bit a 1.4 dB higher SNR is required compared to the simulation without any quantization. The receiver with word length of 8 bit operates already quite well as it exhibits a difference of only 0.6 dB to the ideal case. Word lengths larger than 10 bits provide only a small improvement. To limit the complexity of the receiver a word length of 8 to 10 bits seems to be a good compromise.

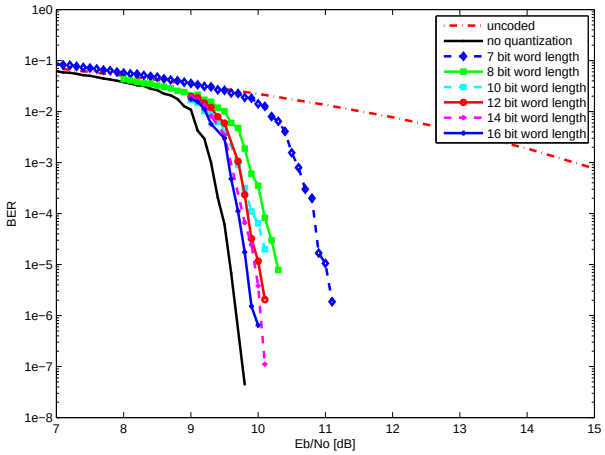

Fig. 7: BER vs. SNR for the EG2m3s3-9of9-ex-CR code using different word length for the arithmetic operations at the receiver. For sampling an ADC with a resolution of 6 bit and uniform quantization is used, while $\Delta\tau = 60\,\mathrm{ps}$ and $R_D = 400\,\mathrm{ps/nm}$.

5 Conclusion

We have examined an optical receiver with electronic detection and LDPC decoding for an optic transmission link. Due to previous findings we restricted our investigations to a receiver with concatenation of the equalizer and decoder without a feedback loop.

Finite geometry LDPC codes with overhead in the range of 6.7 to 14.3 % have been found. They can provide a BER vs. SNR performance close to the capacity bound. Powerfull LDPC codes with overhead of 6.7 % exhibit a high complexity. For a code overhead of 12.5 % and 14.3 % codes with better BER performance and with a two to eight times smaller codeword length were found. Thus they are dedicated for hardware implementation.

For sampling of the electrical receive signal a uniform and nonuniform quantization was considered. For a low resolution of the ADC the nonuniform quantization performs better than the uniform version. However, high FEC performance requires a resolution of 5 or 6 bit. For these resolutions the nonuniform quantization provides no appreciable improvement. Thus an ADC with uniform output levels and a resolution of 5 to 6 bit is preferable. In combination with a word lenght of 8 bit of the arithmetic operations the receiver exhibits a difference of only 0.6 dB compared to a receiver with no quantization.

Finally it can be stated, that a receiver scheme was found, which is dedicated for implementation in hardware. Parallelization of the BCJR equalizer and the SPA decoder enables a bitrate of 10 Gbit/s.

References

[1] J. Hagenauer, “The turbo principle: Tutorial introduction and state of the art,” *Proceedings of the International Symposium on Turbo Codes, Brest, France*, pp. 1–11, Sep. 1997.

[2] M. Jäger, T. Rankl, J. Speidel, H. Bülow, and F. Buchali, “Performance of turbo equalizers for optical PMD channels,” *J. Lightw. Technol.*, vol. 24, no. 3, pp. 1226–1236, Mar. 2006.

[3] H. Haunstein, T. Schorr, A. Zottmann, W. Sauer-Greff, and R. Urbansky, “Performance comparison of MLSE and iterative equalization in FEC systems for PMD channels with respect to implementation complexity,” *J. Lightw. Technol.*, vol. 24, pp. 4047–4054, Nov. 2006.

[4] T. Rankl, “Turbo equalization with convolutional and LDPC codes as well as analytically computed metrics.” Leipzig: 9. ITG-Fachtagung Photonische Netze, Apr. 2008, pp. 165–172.

[5] T. Rankl, C. Kurz, and J. Speidel, “Performance bounds of optical receivers with electronic detection and decoding,” *J. Lightw. Technol.*, vol. 27, no. 16, pp. 3567 – 3579, Aug. 2009.

[6] L. Bahl, J. Cocke, F. Jelinek, and J. Raviv, "Optimal decoding of linear codes for minimizing symbol error rate," *IEEE Trans. Inf. Theory*, vol. 20, pp. 284–287, Mar 1974.

[7] P. Robertson, E. Villebrun, and P. Hoeher, "A comparison of optimal and sub-optimal MAP decoding algorithms operating in the log domain," in *Communications, 1995. ICC '95 Seattle, 'Gateway to Globalization', 1995 IEEE International Conference on*, vol. 2, Jun. 1995, pp. 1009–1013.

[8] A. Worm, H. Lamm, and N. Wehn, "VLSI architectures for high-speed MAP decoders," in *VLSI Design, 2001. Fourteenth International Conference on*, 2001, pp. 446–453.

[9] M. Mansour and N. Shanbhag, "VLSI architectures for SISO-APP decoders," *IEEE Trans. VLSI Syst.*, vol. 11, no. 4, pp. 627– 650, Aug. 2003.

[10] S. Lin, J. Daniel, and J. Costello, *Error control coding*. New York: Prentice Hall, 2005.

[11] T. Brack, F. Kienle, and N. Wehn, "Disclosing the LDPC code decoder design space," in *Design, Automation and Test in Europe, 2006. DATE '06. Proceedings*, vol. 1, Mar. 2006.

[12] G. P. Agrawal, *Nonlinear Fiber Optics*. New York: Academic Press, 1998.

[13] M. Franceschini, G. Bongiorni, G. Ferrari, R. Raheli, F. Meli, and A. Castoldi, "Fundamental limits of electronic signal processing in direct-detection optical communications," *J. Lightw. Technol.*, vol. 25, no. 7, pp. 1742 –1753, Jul. 2007.

[14] Y. Kou, S. Lin, and M. P. C. Fossorier, "Low-density parity-check codes based on finite geometries: A rediscovery and new results," *IEEE Trans. Inf. Theory*, vol. 47, no. 7, pp. 2711–2735, Nov. 2001.

[15] B. Vasic and O. Milenkovic, "Combinatorial constructions of low-density parity-check codes for iterative decoding," *IEEE Trans. Inf. Theory*, vol. 50, pp. 1156 – 1176, Jun. 2004.

[16] H. Bülow and T. Rankl, "Soft decoded modulation for sensitivity enhancement of coherent 100-Gbit/s transmission systems," in *Optical Fiber Communication - incudes post deadline papers, 2009. OFC 2009. Conference on*, Mar. 2009, pp. 1–3, oFC.

[17] F. Lang, T. Alpert, D. Ferenci, M. Grözing, and M. Berroth, "Design of a 25 GS/s 6-bit flash-ADC in 90 nm CMOS technology," in *ESSCIRC 2009 Fringe (European Solid-State Circuits Conference Fringe)*, Sep. 2009.